



ORIGINAL ARTICLE

Optical and electrochemical recognition studies of anions via novel benzothiazole azo-derivative



Ranjeet Kaur^a, Gargi Dhaka^a, Parkash Singh^b, Shweta Rana^{a,*}, Navneet Kaur^{a,*}

^a Department of Chemistry, Panjab University Chandigarh, 160014, India

^b Department of Mechanical Engineering, Malout Institute of Management and Informational Technology, Malout 152107, India

Received 27 March 2020; accepted 12 May 2020

Available online 21 May 2020

KEYWORDS

Benzothiazole;
Computational chemistry;
Electrochemistry;
Multianalyte;
Optical;
Sensing;
Supramolecular chemistry;
Stripping analysis;
Taguchi-method

Abstract Herein, a novel supramolecular probe 4-(2-phenyldiazenyl)-2-(benzothiazol-2-yl) phenol (1) has been described, where assimilation of benzothiazole unit with azo functionality led to innovative electrochemical and optical response towards anions. The successful formation was confirmed using ¹HNMR, ¹³C NMR and HRMS. This rationally planned receptor **1** exhibits multi recognition modes in showing selectivity towards AcO⁻ and F⁻ anions by both visual and absorption processes; while I⁻ is sensed selectively via redox mechanism. The multi recognition mechanisms were thoroughly documented by DFT giving an insight picture of the mode of interaction of the anions in HOMO-LUMO energy levels ultimately affecting the activity of the designed benzothiazole moiety. Optimization of various parameters related to redox response was also analyzed by Taguchi method to minimize the effect of uncontrollable variables. Lower detection limit for the anions by different response mechanisms in a single moiety enhances the future possibility of an economic and time saving multichannel chemosensor.

© 2020 Published by Elsevier B.V. on behalf of King Saud University. This is an open access article under the CC BY-NC-ND license (<http://creativecommons.org/licenses/by-nc-nd/4.0/>).

1. Introduction

Anions play a significant role in various biomolecules such as haemoglobin, chlorophyll, vitamin B12 along with a domineering role in the arena of environmental, biochemical as well as industrial sectors (Chowdhury et al., 2018; Ni et al., 2017;

Xiong et al., 2011). However, apart from their uses, their excessive intake can lead to serious health problems with an increased risk of immune/geno/neurotoxic defects, that ultimately put stress on the design and synthesis of probes capable of selective binding and sensing of these anions (Kumar et al., 2017). These characteristics tend to direct them towards the dome of supramolecular chemistry, which inherits the capability of interaction with these anions (Ghaemi et al., 2014). Benzothiazole (N-containing heterocycle intermediates) based electrochromic scaffolds are most extensively studied groups of supramolecular chemistry as they surrogate for anthraquinone analogues with improved stability, shading the range of their limitations (Maradiya, 2012). Also, benzothiazole containing motifs, exhibit large molecular hyperpolarizability making them imminent competitor as chemosensor for anion

* Corresponding authors.

E-mail addresses: shweta0402@pu.ac.in (S. Rana), neet_chem@pu.ac.in (N. Kaur).

Peer review under responsibility of King Saud University.



sensing (Manuela et al., 2011; Sharma et al., 2015). They possess endocyclic heteroatoms which can lead to excellent ligand properties with distinct donor abilities (Zeng et al., 2019). The use of aryl and heteroaryl diazenes in conjugation with benzothiazole has sought their use as a second harmonic generation chromophores (Hrobarikova et al., 2010; Su et al., 2014).

Introduction of diverse functionalities in benzothiazole, have been reported earlier, for screening of anions via deep absorption modes (Keshav et al., 2017; Padghan et al., 2016; Vidya et al., 2017). Li et al. have designed benzothiazole based fluorescent probe for Zn^{2+} and Cd^{2+} ions, where modification of surface of benzothiazole with auxiliary ligand cysteine, has led to their discrimination by shift in peak positions (Li et al., 2018). Kaur et al. 2018 have synthesized 2-(4-amino-2-hydroxy phenyl)benzothiazole based Schiff base which exhibit selective response towards HSO_4^- and I^- (Kaur et al., 2018). In view of advancing sensor technology, considerable attention has also been paid in the synthesis of redox active receptors, that enclose redox center in the vicinity of guest binding site (Shu and Tang, 2020; Lv et al., 2020). The benzothiazole unit consists of fused rings structure with π -type orbital arrangement in molecules, resulting in lower band gaps which pose excellent electronic conductance in such molecules (Chen et al., 2014). The binding of anion, prompts a positive or negative shift in the redox potential of probe and the magnitude of the electrochemical shift epitomizes a quantitative analysis of agitation of redox center prompted by complexation to the receptor unit. Sharma et al. have exploited this attribute in benzimidazole/benzothiazole based electrochemical sensor for nanomolar detection of guanine (Sharma et al., 2015).

Using this keystone as the basis of such precedents, a suitable multisignalling chemical probe can be designed by combining redox activity of benzothiazole unit with optical recognition properties of its derivatives. Considering the demand of latest technology, multiple analyte sensing offered by a single probe is economical and time saving. Although, few reports based on this kind of multirecognition modes are available in literature (Ebaston et al., 2016; Manna et al., 2019; Gupta et al., 2016), but to the best of our knowledge, the multirecognition mode analysis for benzothiazole scaffolds have not been explored yet. The benzothiazole moiety is an interesting electrochromic moiety possessing multisignalling behavior of all visual, optical and redox sensing in a single moiety. Therefore here, to extend it further we have anticipated that assimilation of benzothiazole unit with diazo compounds will lead to innovative multisignalling sensing attributes comprising of both electrochemical and optical ones. The designed sensor has been thoroughly evaluated for multi-channel modes experimentally as well as theoretically with detailed optimizations showing sensing for different anions with different physical outputs incorporated into a single moiety.

2. Experimental

2.1. Materials & instrumentation

All the chemicals and solvents were purchased from Sigma-Aldrich Chemical Co. and were used without further purification. Deionized water was used throughout the experiments. Acetonitrile (CH_3CN) used in the experiments was of high per-

formance liquid chromatography (HPLC) grade. 1H and ^{13}C nuclear magnetic resonance (NMR) spectra were achieved on a BRUKER AVANCE II FT NMR (400 MHz) spectrophotometer and BRUKER AVANCE II FT NMR (100 MHz) spectrophotometer using tetramethylsilane (TMS) as an internal standard and dimethyl sulphoxide ($DMSO-d_6$) as a solvent. The chemical shifts are reported in δ (ppm). Purification and separations by column chromatography were performed on silica gel, using normal or flash chromatography. The ultraviolet-visible (UV-VIS) spectra were recorded in a JASCO V-530 UV-VIS spectrophotometer from 200 to 900 nm range. All the anions (F^- , Cl^- , Br^- , I^- , AcO^- and HSO_4^-) were prepared in distilled CH_3CN as their tetrabutylammonium salts. All the electrochemical measurements were performed using Autolab/PSTAT204N at room temperature in three electrode setup with Au electrode as working electrode, Ag/AgCl as reference electrode can be utilized as the long term exposures are avoided in this case while platinum as counter to eliminate extra currents in the system. The square wave anodic stripping voltammograms (SWASV) were carried out at deposition potential of + 0.8 V and deposition time of 25 s and thereafter stripping was carried out in the region of + 0.3 V to + 1.2 V with amplitude 50 mV and frequency 25 Hz.

2.2. Synthesis of 4-(2-phenyldiazenyl)-2-(benzothiazol-2-yl)phenol (chemosensor 1)

In a round bottom flask (RBF, 100 mL), aniline (0.094 g, 1 mmol) was suspended in 30.0 mL of distilled water at the temperature of 0–5 °C. Then 1.0 mL of HCl solution was added to the mixture. After 15 min, aqueous solution of sodium nitrite (0.076 g, 1.1 mmol) was added, followed by THF solution of 2-(2'-hydroxyphenyl)benzothiazole (0.227 g, 1 mmol), then pH was adjusted to 8–9 with NaOH solution. After stirring for 4 h, the solution was neutralized with HCl solution. The produced precipitate was filtered and washed several times with water and dried at vacuum. Column chromatography, in hexane-ethyl acetate solvent system, was performed to obtain pure azo compound **1** in a yield of 60%. Solid, Mp (°C) 140, Yield (%) 68; 1H NMR ($CDCl_3$, 400 MHz) δ (ppm): 7.24 (t, 1H, $J_1, J_2 = 8.0$ Hz, Ar-H), 7.44 (d, 1H, $J = 8.0$ Hz, Ar-H), 7.48 (d, 1H, $J = 8.0$ Hz, Ar-H), 7.53 (t, 3H, $J_1, J_2 = 8.0$ Hz, Ar-H), 7.94 (t, 3H, $J_1, J_2 = 8.0$ Hz, Ar-H), 8.04 (d, 2H, $J = 8.0$ Hz, Ar-H), 8.34 (s, 1H, Ar-H), 13.0 (s, 1H, Phenolic -OH); ^{13}C NMR ($CDCl_3$, 100 MHz) δ (ppm): 168.9, 160.6, 152.6, 151.6, 145.8, 132.8, 130.7, 129.1, 126.9, 125.9, 124.9, 122.7, 122.3, 121.7, 118.7, 116.8; ESI-MS: m/z (relative abundance (%), assignment) = 332.0338 [100, (M + 1) $^+$].

2.3. Anion recognition experiments

For titrimetric experiments, stock solutions of the chemosensor **1** (10^{-2} M) and different ions (10^{-1} M) were prepared in DMSO and were diluted accordingly to carry out spectrophotometric and electrochemical analysis. The sensing analysis was performed in distilled CH_3CN with 10 μ M solution of chemosensor **1** by adding 100 equivalents of different anions. The complete coordination was ensured by keeping anion-chemosensor **1** solutions for some time. The differences among the spectral behavior of various anions were monitored using

UV–VIS spectroscopy and also limits of detection were calculated by standard analytical procedure. Also, the electrochemical response was analyzed in similar way using chemosensor **1** (0.1 mM) and 100 equivalents of different anions with square wave anodic stripping voltammetry (SWASV). The deposition of anions was obtained by applying fixed reduction potentials. The stripping curve was noticed in the region of +0.3 V to +1.2 V wherein Au-electrode serving as working electrode.

2.4. Titration measurements

Titration experiments were performed in similar way using distilled CH₃CN with chemosensor **1** (10 μM). The different analytical curves like Job's plot and binding isotherms were obtained by adding different aliquots of (0–30 equivalent) of anions. Similarly, electrochemical measurements were also performed in distilled CH₃CN solution containing lithium trifluoromethanesulfonate as an electrolyte. The titration experiments for redox analysis were done in 0.1 mM of chemosensor **1**, containing different concentrations of I⁻ ion (stock 10⁻¹ M) and corresponding current was noted down using SWASV. Prior to each analytical curve measurement, working electrode (Au electrode) was polished with alumina slurry and subsequently washed with deionized water.

2.5. Quantum mechanical calculations

The density functional theory (DFT) calculations and structure optimizations were carried out using DFT/B3LYP-6-31G and 3–21 G basis set. The geometry of synthesized probe was optimized using above said basis set for proper assignment of all the energy states involved during the whole process. All of the calculations were performed on Gaussian 09 package.

2.6. Optimization using TAGUCHI method

In order to account for the behavior of deposition potential and deposition time along with effect of changing anion, analysis of current response by Taguchi method was done. For this, L25 orthogonal array was selected using MINITAB18 and the design of experiment (DOE) was prepared. The respective values of responses were written according to the DOE in MINITAB18 and the main effect plot for S/N ratios of each factor at the each level were plotted with the help of MINITAB18 software. The optimized parameters obtained for maximum current response were then compared with experimental studies and are then utilized for further studies.

3. Results and discussion

3.1. Synthesis of chemosensor **1**

Scheme 1 outlines the synthesis of the azo derivative chemosensor **1**, where azo coupling reaction of 2-(2'-hydroxy phenyl) benzothiazole with aniline resulted in formation of chemosensor **1** (Pan et al., 2017). ¹H NMR, ¹³C NMR and ESI-MS spectra of chemosensor **1** are shown in **Fig. S1** to **S3** in the **Supporting Information (SI)**.

3.2. Spectrophotometric analysis and visual recognition of chemosensor **1** with anions and their density functional theory (DFT) studies

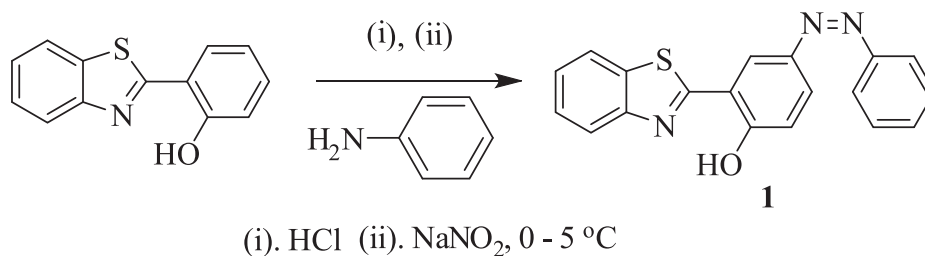
As phenolic –OH is well known for its interaction with anions, so the optical responses of chemosensor **1** towards various anions viz. AcO⁻, F⁻, Cl⁻, Br⁻, I⁻ and HSO₄⁻ ions using tetrabutyl ammonium as the counter cation, were explored by monitoring the color changes. The colorimetric monitoring was primarily done by adding 100 equivalents of various anions viz. AcO⁻, F⁻, Cl⁻, Br⁻, I⁻ and HSO₄⁻ ions to 10 μM solution of chemosensor **1** in CH₃CN. With addition of AcO⁻ and F⁻ ions to CH₃CN solution of chemosensor **1**, conspicuous color change from colorless to respective orange and yellow color was observed (inset **Fig. 1**). These studies indicated that chemosensor **1** could be employed as an efficient receptor for colorimetric sensing of AcO⁻, and F⁻ ions.

The UV–VIS. absorption spectra of chemosensor **1** (10 μM), in CH₃CN, exhibited dual absorption bands; one at lower wavelength at 318 nm (in chemosensor **1**) due to coupled thiazole and fused phenyl ring and another band at a longer wavelength of 343 nm corresponded to the coupled benzothiazole and the hydroxyphenyl ring. The anion binding abilities of chemosensor **1** have been evaluated in CH₃CN solution, by adding 100 equiv. of the tetrabutylammonium salts of various anions such as F⁻, Cl⁻, Br⁻, I⁻, HSO₄⁻ and AcO⁻ (**Fig. 1**). Here, addition of AcO⁻ and F⁻ ions caused absorption changes i.e. emergence of a new absorption band at longer wavelength (470 nm); while absorption spectra of chemosensor **1** changed negligibly with addition of rest of anions.

To enumerate the cause for visible color change, the UV–VIS. absorption spectral titrations of chemosensor **1** were carried out by progressive addition of AcO⁻/F⁻ ions in CH₃CN solution (**Fig. 2(a,b)**). The receptor peak of chemosensor **1** was characterized by the appearance of two bands centered at 318 and 343 nm. As shown in **Fig. 2(a)**, upon gradual increase of the AcO⁻ ion (0–30 equiv.), the bands at 318 and 343 nm decreased in intensity and a new band appeared at 470 nm with an isosbestic point at 375 nm. The ratiometric curve of the absorption spectra with isosbestic point indicated the formation of a new intermolecular charge transfer complex between the receptor (chemosensor **1**) and AcO⁻ ion, which was responsible for the visible color change from colorless to orange inset (**Fig. 1**).

The deprotonation of phenolic –OH ascribed to strong hydrogen bonding interaction between chemosensor **1** and AcO⁻ has enhanced < pi > delocalization, which decreases the energy of the π → π* transition. This has been accounted with the help of appearance of a new absorption band near 470 nm resulting in the formation of naked eye orange color (**Fig. 3**). As a consequence, the electronic properties of chemosensor will result in the visible color changes and appearance of new band at longer wavelength.

Similar UV–VIS. spectral observations were obtained when F⁻ (**Fig. 2(b)**) ions were added separately in CH₃CN solution of chemosensor **1** (10 μM). Here also, the ratiometric curve of the absorption spectra was observed for F⁻ ions, indicating the formation of a new intermolecular charge transfer complexes between the chemosensor **1** and F⁻ ions (**Fig. 4(b)**).



Scheme 1 Synthetic protocol to generate target chemosensor **1**.

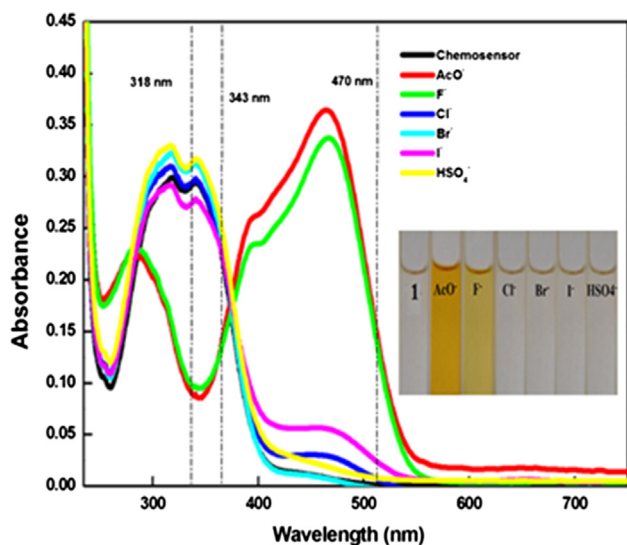


Fig. 1 UV-VIS. absorption spectra of chemosensor **1** (10 μ M) upon addition of 100 equiv. of various anions as their tetrabutyl ammonium salts in CH₃CN, with inset showing the colorimetric analysis of chemosensor **1** (10 μ M) with 100 equiv. of diverse anions in CH₃CN.

The binding stoichiometry of chemosensor **1** and AcO⁻/F⁻ were supported by Job's plot according to the continuous variations method that indicated the 1:1 interaction between

sensed anions (AcO⁻/F⁻) and chemosensor **1** (Fig. S(4)). The association constant of chemosensor **1** with AcO⁻ was calculated based on the UV-VIS titration through the Benesi-Hildebrand equation which is given as follows (Vashisht et al., 2019):

$$\frac{1}{A - A_0} = \frac{1}{A_{\max} - A_0} + \frac{1}{[A_{\max} - A_0]K[C]} \quad (1)$$

here, A₀, A, and A_{max} is the absorbance of free chemosensor **1**, measured with AcO⁻ and measured with excess amount of AcO⁻ at 470 nm, respectively and K is the association constant and [C] is the concentration of AcO⁻ ion added. Plotting of 1/(A - A₀) versus 1/[AcO⁻] showed a linear relationship, which indicates that chemosensor **1** associates with AcO⁻ in a 1:1 stoichiometry, as earlier indicated by Job's plot. The binding constant (K) between chemosensor **1** and AcO⁻ is determined from the ratio of intercept/slope to be 2.8 × 10⁵ M⁻¹. The binding constants of chemosensor **1** with F⁻ ions were found to be 1.3 × 10⁵ M⁻¹ which is far more than already reported methods.

The limit of detection of chemosensor **1** was calculated from the linear part of the curve plotted between the concentration of analyte vs. corresponding absorption and emission intensity (Dhaka et al., 2017). From this, the limits of detection for various anions as AcO⁻ and F⁻ ions were estimated to be 84 μ M and 53 μ M respectively, via UV-VIS absorbance studies for chemosensor **1** which is comparable to already reported methods (Panitsiri et al., 2016). The selectivity of chemosensor **1**

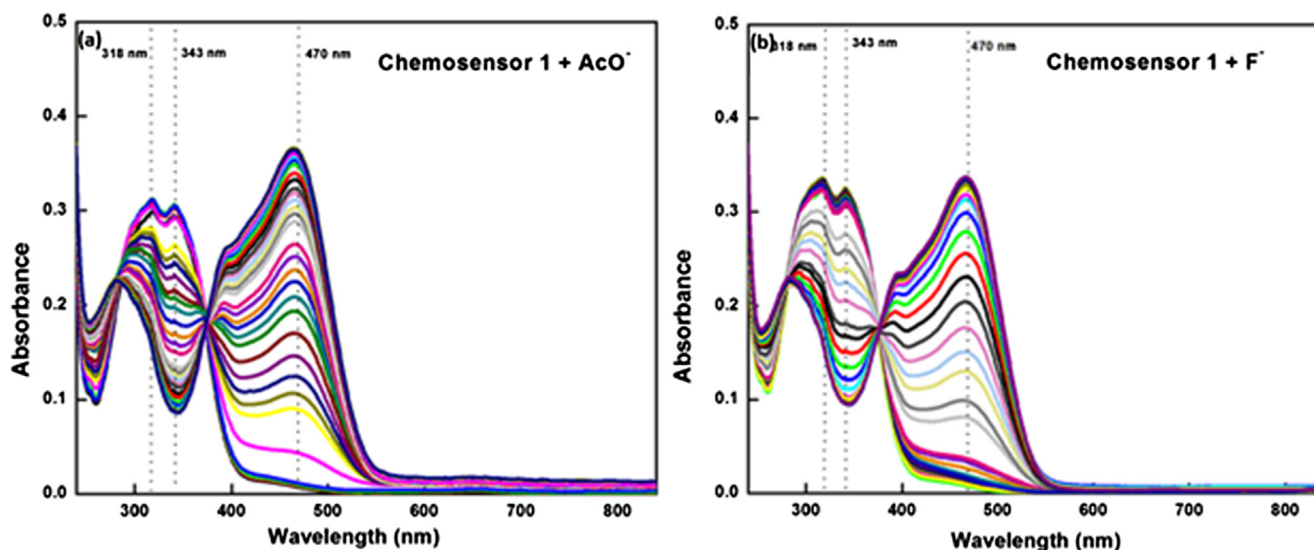


Fig. 2 UV-VIS. spectra of chemosensor **1** (10 μ M) upon addition of (a) AcO⁻ from 0.1 to 30 equiv. (b) F⁻; 0.1 to 20 equivalent.

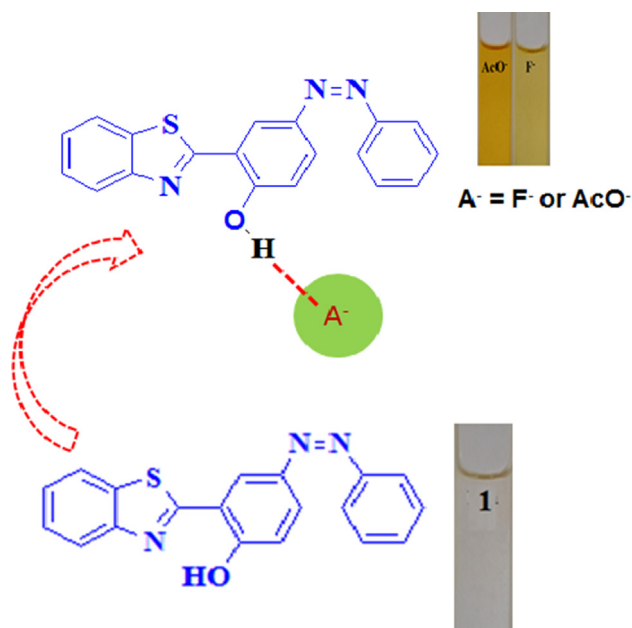


Fig. 3 Possible sensing mechanism for sensing of anions.

was also endorsed towards AcO^- and F^- ions in the presence of various interfering ions (Cl^- , Br^- , I^- and HSO_4^-) and in each other's presence, by using UV-VIS absorption spectroscopy. 100 equiv. of aforementioned ions were added to **1**. AcO^-/F^- (10 μM of **1** with 10 added equiv. of AcO^-/F^-) acetonitrile solution. The bar graphs (Fig. 5(a,b)) clearly represent the non-interference of various anions in the recognition process. The least interference was observed in both cases leading to anti-interfering ability of prepared chemosensor.

To check the structural features and account for the proposed mechanism, computational analysis of the chemosensor **1** was carried out with AcO^- ions. The optimization of structure of chemosensor **1** and the 1:1 species with AcO^- ions were optimized by DFT method and in order to further recognize the behavior of AcO^- ions with the

chemosensor **1**, the DFT calculations have been carried out. The structures of the chemosensor **1** and its chemosensor **1**: AcO^- complex were optimized using the Gaussian 09 package using the exchange correlation function B3LYP and the basis sets 6-31G (d,p) for C, H, N and O atoms.

The energy comparison diagram (Fig. 6) depicted that on complexation of chemosensor **1** with AcO^- ions, the calculated energy gap of HOMO and LUMO decreased with respect to free chemosensor indicating the formation of stable complex and corroborating for the red shift in the UV-vis spectrum. In chemosensor **1**, only one AcO^- ion binds to the $-\text{OH}$ with simultaneous longer distance overlap between the orbitals of the metal ion justifying the experimental 1:1 stoichiometric ratio. The electron density of the HOMO and LUMO of chemosensor **1** lies on the electron withdrawing part of the respective ligands. The contour plots of the HOMO after the addition of AcO^- ions showed that the electron density is over the acetate ion itself. However, the electron density of the LUMO was situated on the electron withdrawing part.

3.3. Electrochemical studies of chemosensor **1** with anions and their density functional theory (DFT) studies:

The square wave anodic stripping voltammetry (SWASV) was done in chemosensor **1** by adding 100 equivalents of various anions i.e. I^- , F^- , Cl^- , Br^- , AcO^- , HSO_4^- to distilled CH_3CN on the surface of Au electrode in the potential range of + 0.3 V to + 1.2 V at amplitude of 50 mV and frequency 25 Hz. After noting down the stripping response, it was observed that in the applied potential range appreciable electrochemical change was observed only for I^- in contrary to the optical results where complete specificity was absent (Fig. 7). The appearance of new oxidation peak after the addition of I^- ion indicates the electron transfer between the receptor and the analyte (Fig. S5).

In the absence of I^- (Fig. 8), chemosensor **1** exhibits oxidation peak at + 1.5 V that is attributed to the presence of benzothiazole moiety with perceptible cathodic peaks at + 0.9 V and at + 0.2 V. The first reduction peak corresponds to the formation of amine group, as most of the azo dyes get reduced

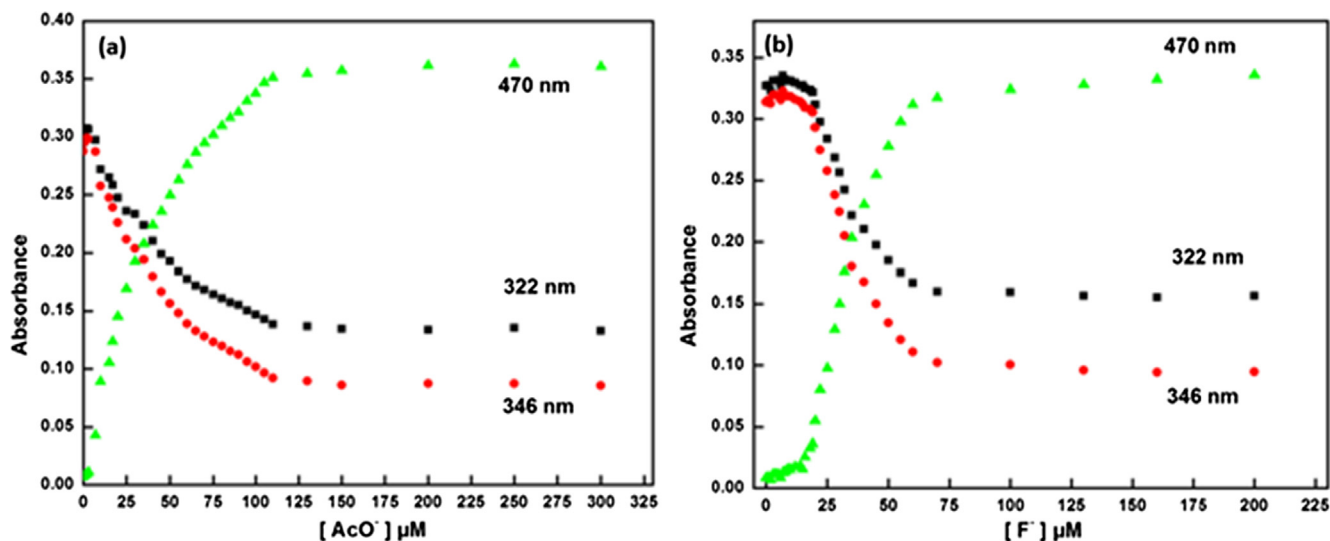


Fig. 4 Binding isotherms of (a) AcO^- and (b) F^- ions at wavelengths of 470, 318 and 343 nm.

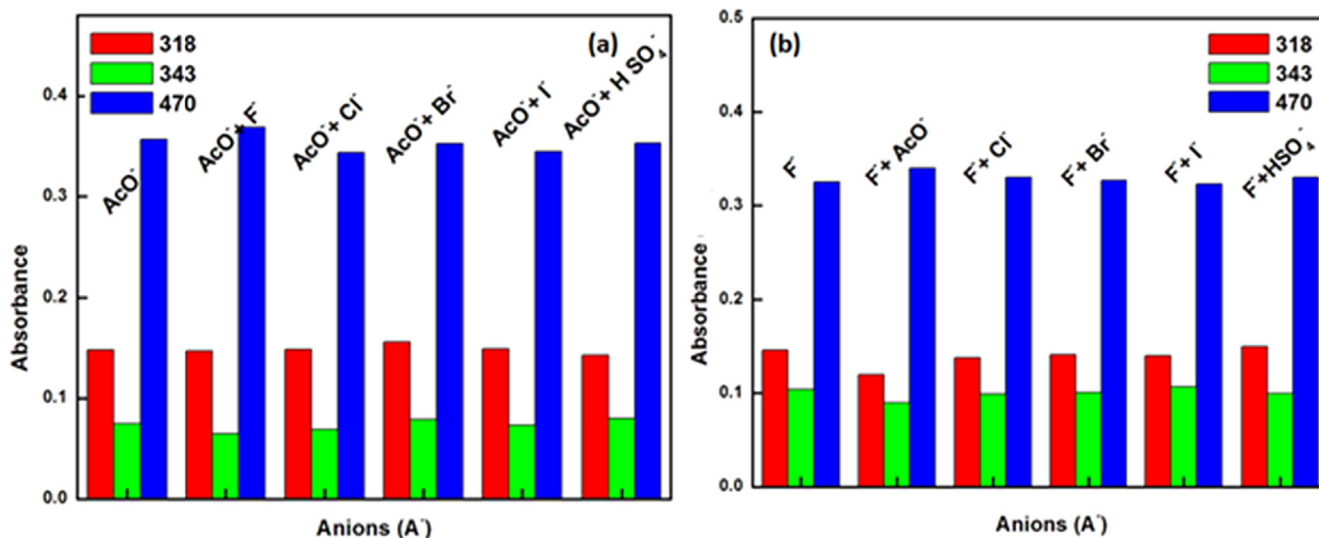


Fig. 5 The effect of various anions on absorption spectra of (a) F⁻ ion (b) AcO⁻

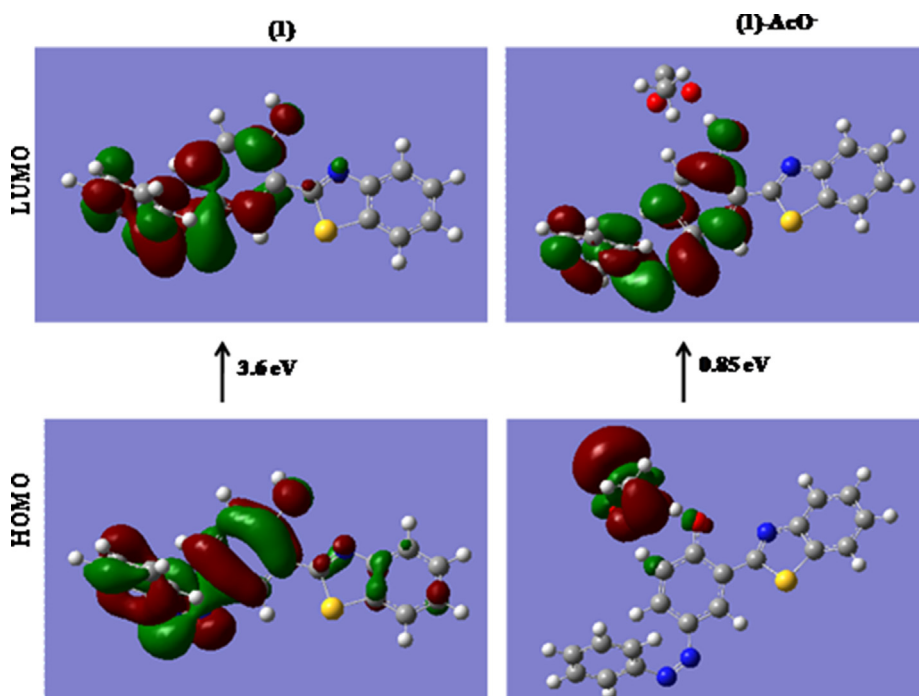


Fig. 6 DFT computed energy level diagrams of HOMO and LUMO of (a) chemosensor 1 (b) chemosensor 1 with AcO⁻

within the potential range of + 0.45 to -1.0 V whereas the second reduction peak is due to formation of hydrazone derivatives (Fierro et al., 2013; Özkütük et al., 2016). After addition of I⁻, it is the I⁻ ion which undergoes oxidation as also inferred from its density functional theory (DFT) studies described later in this section.

These compounds absorb electrons of energy equal to or higher than the band gap resulting in excitation of electron from HOMO to LUMO level which is helpful in designing the redox sensing system. As oxidation involves the loss of electrons, onset oxidation potential (E_{ox}) corresponds to ionization potential whereas onset reduction potential (E_{red}) rela-

tive to an Ag reference electrode, corresponds to electron affinity thus correlated with LUMO. The band gap is deduced from the energy of conduction and valence band using the equation 6 that comes out to be 3.6 eV while after the addition of iodide ion the band gap value lowers down to approximately 1.59 eV (Leonat et al., 2013).

$$E_{HOMO} = -(E_{ox} + 4.4)eV \text{ and } E_{LUMO} = -(E_{red} + 4.4)eV \quad (2)$$

Molecular orbital study can also be used to understand the mode of interaction and contribution of I⁻ ion in HOMO-LUMO energy level that will affect the redox potentials and chemical activity of benzothiazole moiety. For this, DFT cal-

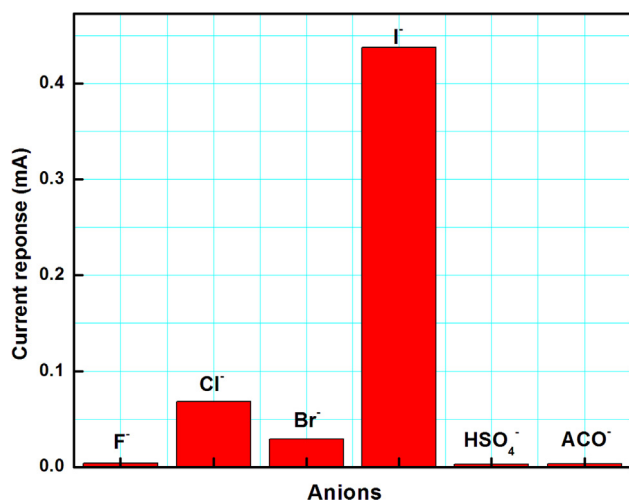


Fig. 7 Changes in SWASV response after the addition of 100 equivalents of anions in distilled CH₃CN (0.1 mM chemosensor 1).

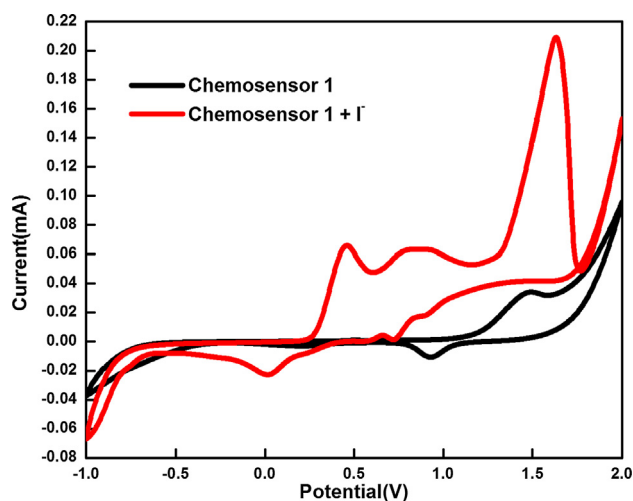


Fig. 8 Cyclic voltammograms of chemosensor 1 in CH₃CN (0.1 mM) using lithium trifluoromethanesulfonate as an electrolyte at scan rate of 100 mV/s in presence and absence of I⁻.

culations were carried out using DFT/B3LYP-6-31G and 3–21 G basis set. The geometry of synthesized probe was optimized using above said basis set for proper assignment of all the energy states involved during the whole process. It is clear that in the ground state optimized geometry, the phenyl ring is twisted w.r.t. benzothiazole unit. The calculated HOMO-LUMO gaps for optimized structure are 3.6 eV and 1.59 eV respectively which decrease in the presence of I⁻, owing to easy electron availability of iodide due to which it gets excited first and undergoes oxidation after acquiring sufficient potential. In the absence of I⁻ ion, the electronic density in HOMO and LUMO of probe are mainly located on azo group indicating it to be most chemically active during the whole electrochemical process as shown in Fig. 9. The electrochemical oxidations and reductions are assigned to that part of moiety which undergoes exchange of electron between HOMO-LUMO under the effect of applied potential as also perceptible in their cyclic voltammograms. Also, the energy gap between the

HOMO-LUMO of molecule is quite large so, the excitation of electron occur at the higher potential and oxidation starts followed by two reductions. After approach of I⁻ molecule, the whole energy density of HOMO of system under investigation is on I⁻ molecule. The I⁻ molecule on oxidation generates electrochemical signals as shown in cyclic voltammograms of system under investigation (Vidya et al., 2017). Also, the present results depicts that the oxidation of I⁻ will precede oxidation of chemosensor 1 and reduction of chemosensor will precede the reduction of iodide ions.

3.4. Taguchi array analysis of the SWASV optimization studies:

The effect of metal ions I⁻, F⁻, Cl⁻, Br⁻, HSO₄⁻ are investigated in Taguchi analysis and it was found that I⁻ imparts maximum changes in amperometric response of chemosensor 1. In redox studies, optimization of deposition potential and deposition time are the key parameters to eliminate the factors causing analytical errors. During optimization using SWASV, it was found that the present method works better at potential of + 0.8 V which is attributed to inadequate oxidation at less positive potentials (Fig. 10a) and oxidation interference from other anions at towards more positive side. After this, deposition time was optimized and it was found that maximum amperometric response is at the time of 25 s (Fig. 10b). The same experiments have been run on MINITAB18 using Taguchi method to evaluate the effect of changing anions, deposition potential and deposition time in order to attain the desired optimal response value for reducing the negative effect of uncontrollable variables (Davis and Pretesh, 2018).

From the plots for S/N ratio the effect of various parameters on changing the above conditions is depicted in the Fig. 10 (c). The current response here in the experiment is “larger-the-better” type quality characteristic giving a mixed scenario for various anions whereas the value of S/N ratio is maximum for iodide.

Also, it can be inferred from S/N ratio plot for current response that as the deposition potential increases from (+0.4 to + 1.2 V), there is a very small impact on the current response. From the main effects plot for S/N ratio, the third level (I⁻) of anions, first level (+0.4 V) of potential, second level (25 s) of the deposition time results in maximum value of current response. Consequently, the optimal factor/level combinations for anions, deposition potential & deposition time respectively were approved for maximum current response. Table S1 shows the analysis of variance for S/N ratio of current response in which the P value and percentage contribution (P_c) are shown.

The following conclusions can be drawn from the ANOVA table of S/N ratio:

- The percentage contribution of anions, potential and deposition time for current responses were 99.93, 0.008 and 0.042%.
- As it can be seen from the ANOVA table that the anions and deposition time are significant parameters instead of having the less percentage contribution of deposition time.

Table S2 shows the response table for S/N ratio for current response which is based on the delta value (difference between the maximum of minimum value of S/N ratio) for that particular parameter. Hence on the behalf of delta value the ranking

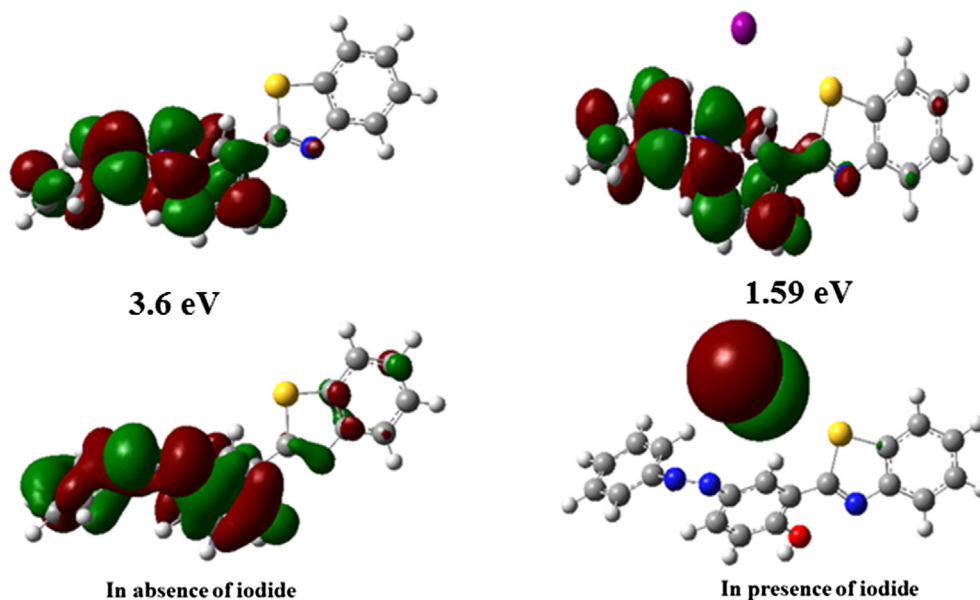


Fig. 9 Electron density mapping and corresponding band gaps of (a) chemosensor **1** (b) chemosensor **1** + Γ^- using DFT/B3LYP-6-31G and 3-21 G basis set.

will start from metal ion followed by deposition time and deposition potential. Here in the experiment the anions are qualitative factors so the conditional/individual regression equation has been drawn for each metal ion as shown in [Table 1](#).

Therefore, based on SWASV and Taguchi analysis the best optimized parameters for response studies are + 0.8 V and 25 s.

3.5. Analytical response towards Γ^-

To check the authenticity and account for the interaction behavior of chemosensor **1** with analyte, titration studies were performed between chemosensor **1** and Γ^- using SWASV. The SWASV sensing involves the following mechanism under consideration during accumulation and stripping ([Guanghan et al., 1995](#); [Souza et al., 2013](#)):



After successful deposition of Γ^- , the stripping was carried out and oxidation peak was observed that is attributed to oxidation of Γ_3^- .



To test the validity of described method for assay of Γ^- ion, evaluation was done by analyzing the peak current values against concentration of Γ^- (5×10^{-4} mM to 1 mM) that exhibits a linear variation [Fig. 11](#) (a). The designed matrix for electrochemical detection of Γ^- is shown to exhibit two linear ranges between 5×10^{-4} mM to 0.075 mM and 0.1 M to 1 mM with the limit of detection of 12.84 μ M and 179.8 μ M. The limit of detection attained using this method is comparable to those already reported chemical sensor with least standard deviations in measurements as compared to already reported methods ([Dielacher et al., 2015](#); [Fierro et al, 2013](#); [Rastegarzadeh et al., 2009](#)) showing the better sensitivity of

the method. Besides these, the quantitative values of sensitivity are of the order of 2.16 and 0.203 mA/mM in the linear range of 5×10^{-4} mM to 0.075 mM and 0.1 M to 1 mM showing wide linear range in different concentrations. This shows the applicability of chemosensor **1** over wide linear ranges. The characteristics of the calibration plot are shown in the [Table 2](#) below:

The reproducibility of chemosensor **1** was checked for seven different solutions (**0.1 mM**) and corresponding current response were evaluated for same concentrations of Γ^- (10 mM) under the optimized conditions. Satisfactory relative standard deviations (RSD) for these measurements of about 0.15% indicate acceptable reproducibility of chemosensor **1**.

The optimized method was tested for interference from various anions (F^- , Cl^- , Br^- , AcO^- , HSO_4^-) and the comparative analysis was done using the equation:

$$\text{Interference}(\%) = (I_0 - I)/I_0 \quad (5)$$

where, I_0 refers to the peak current for Γ^- ion and I refers to the peak current for Γ^- and the interferences. There is no significant interference from F^- whereas upto 50% inference was observed from Br^- and Cl^- as these ions form complex anion with iodine as I_2Br , I_2Cl . Therefore, it is inferred that this method poses the limitation of interference from these anions ([Table 3](#)).

4. Conclusions

A novel electrochromic chemosensor 4-(2-phenyldiazenyl)-2-(benzothiazol-2-yl) phenol (**1**), offering the benefit of multi-recognition modes for different anions in a single moiety has been successfully synthesized. The computational analysis corroborating with the optical and electrochemical data gives an insight view of the sensing mechanism which is quite significant in the development of technology. The chemosensor **1** exhibited multifaceted analysis of AcO^- and F^- with lower limit of

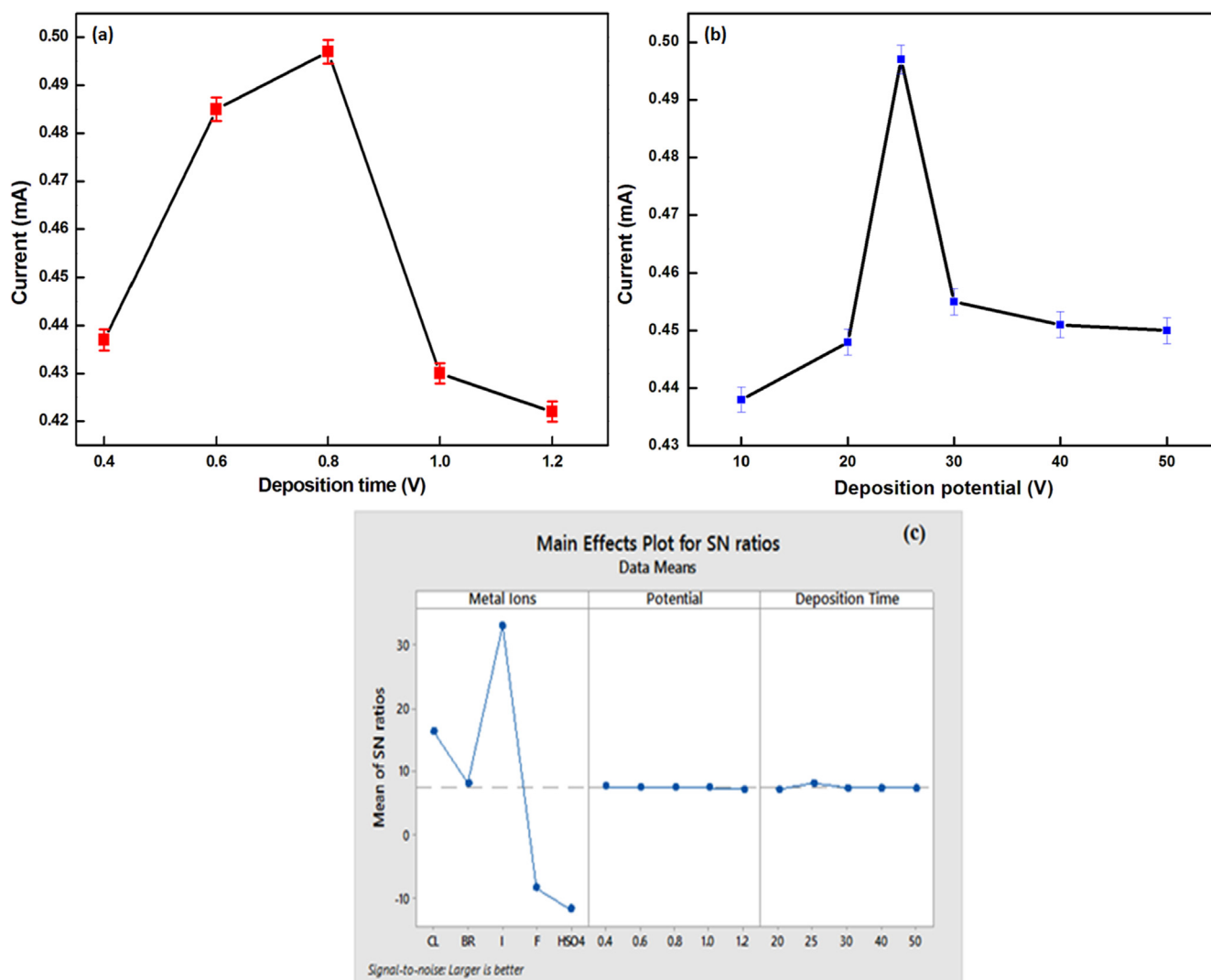


Fig. 10 Optimization of (a) deposition potential (b) deposition time using 100 equivalent of iodide at amplitude of 50 mV and frequency of 25 Hz (c) Main effects plot for S/N ratio of current response.

Table 1 The regression equations corresponding to different anions at different deposition potentials and deposition time.

Cl ⁻	Current (in e-5)	=	6.724-0.389 deposition potential + 0.00245 Deposition Time
Br ⁻	Current (in e-5)	=	2.784-0.389 deposition potential + 0.00245 Deposition Time
I ⁻	Current (in e-5)	=	45.110-0.389 deposition potential + 0.00245 Deposition Time
F ⁻	Current (in e-5)	=	0.611-0.389 deposition potential + 0.00245 Deposition Time
HSO ₄ ⁻	Current (in e-5)	=	0.489-0.389 deposition potential + 0.00245 Deposition Time

detections (84 μM and 53 μM respectively), via visual recognition and absorbance studies as well as selective response towards I⁻ with limit of detection of 12.84 μM as measured by SWASV. The analytical response in all the signaling approaches is significantly better than the already reported multisignalling chemosensors showing an example of good synergy in output response. Apart from sensitivity, the

chemosensor also exhibits the benefits of high ion selectivity in the coexistence of other anions, has wide working range and good reproducibility making it a pertinent candidate for multisignal based ion sensing electrode material. This inexpensive and time saving technology has the immense potential for future practical device applications if coupled with solid state matrices.

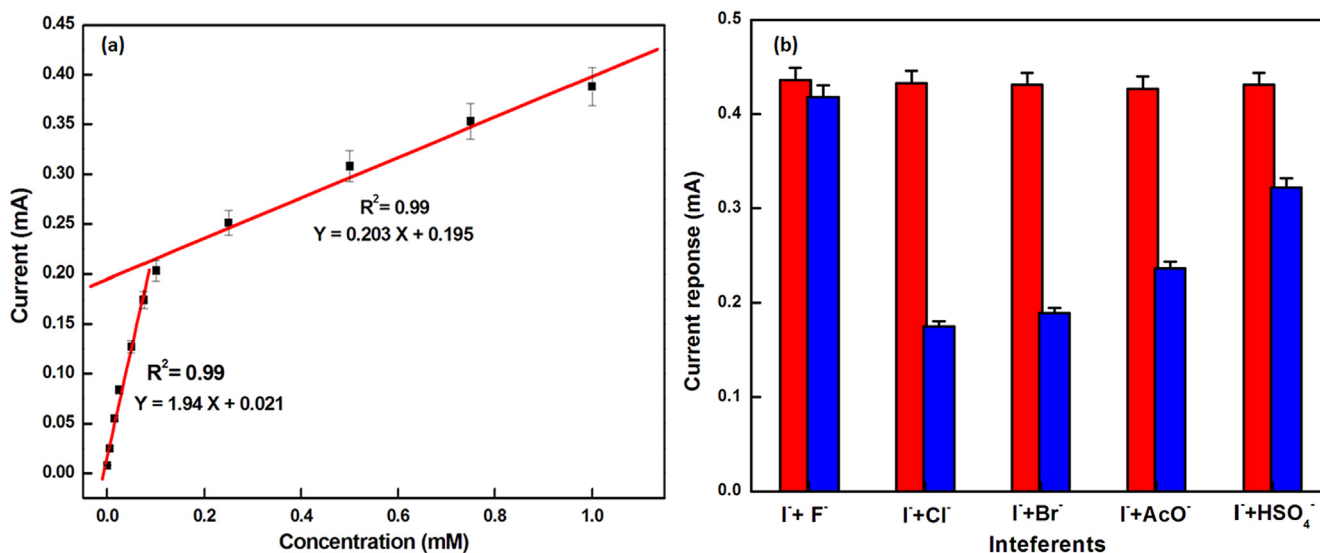


Fig. 11 (a) Linear relationship between stripping current and concentration of I⁻ obtained SWASV for the detection of I⁻ for concentrations 5×10^{-4} mM to 1 mM of iodide solution at 50 mV amplitude and frequency of 25 Hz in CH₃CN using lithium trifluoromethanesulfonate as an electrolyte and (b) Current response after the addition of 100 equivalents of interfering anions in distilled CH₃CN (0.1 mM chemosensor **1**) and (10 mM) of I⁻.

Table 2 Different parameters obtained from calibration plot of peak current vs. concentration of I⁻.

Parameters	Lower range	Upper range
Slope	2.16	0.203
Intercept	0.0172	0.195
Standard deviation (S.D.)	0.00925	0.01217
Correlation coefficient (R)	0.99	0.99
Limit of Quantification (LOQ)	42.8 μ M	599 μ M
Sensitivity (mA/mM)	2.16	0.203
Limit of detection (LOD)	12.84 μ M	179.8 μ M

Table 3 Interference study of various anions towards SWASV of 100 equivalent of iodide ion.

S. No.	Metal ion	Concentration of interfering ion	Interference (%)
1.	F ⁻	1:1	4.13
2.	Cl ⁻	1:1	59.34
3.	Br ⁻	1:1	56.14
4.	AcO ⁻	1:1	44.73
6.	HSO ₄ ⁻	1:1	25.27

Conflicts of interest

The authors declare no conflicts of interest.

Acknowledgements

Financial grant from Department of Science and Technology-Science and Engineering Research Board (Grant No. SERB/2016/000046) is gratefully acknowledged by the authors. Ranjeet Kaur acknowledges council of scientific and

industrial research (CSIR, File no. 09/135(0826)/2018-EMR-I) for senior research fellowship (SRF).

Appendix A. Supplementary material

Supplementary data to this article can be found online at <https://doi.org/10.1016/j.arabjc.2020.05.018>.

References

- Chen, C.J., Smeu, M., Ratner, M.A., 2014. Modeling ion sensing in molecular electronics. *J. Chem. Phys.* 140 (5), 054709–054716.
- Chowdhury, S., Rooj, B., Dutta, A., Mandal, U., 2018. Review on recent advances in metal ions sensing using different fluorescent probes. *J. Fluorescence* 28 (4), 999–1021.
- Davis, R., Pretesh, J., 2018. Statistical Approaches With Emphasis on Design of Experiments Applied to Chemical Processes. <https://doi.org/10.5772/intechopen.69501>.
- Dhaka, G., Kaur, N., Singh, J., 2017. Luminescent benzothiazole-based fluorophore of anisidine scaffolds: a “turn-on” fluorescent probe for Al³⁺ and Hg²⁺ ions. *J. Fluorescence* 27 (6), 1943–1948.
- Dielacher, B., Tiefenauer, R.F., Junesch, J., Vörös, J., 2015. Iodide sensing via electrochemical etching of ultrathin gold films. *Nanotechnology* 26 (2), 025202–025213.
- Eboston, T.M., Balamurugan, G., Velmathi, S., 2016. A fluorogenic and chromogenic dual sensor for the detection of cyanide and copper(II) in water samples and living cells. *Anal. Methods* 8 (38), 6909–6915.
- Fierro, S., Cominellis, C., Einaga, Y., 2013. Simultaneous detection of iodine and iodide on boron doped diamond electrodes. *Talanta* 103, 33–37.
- Ghaemi, A., Tavakkoli, H., Mombeni, T., 2014. Fabrication of a highly selective cadmium (II) sensor based on 1,13-bis(8-quinolyl)-1,4,7,10,13-penta-oxatridecane as a supramolecular ionophore. *Mater. Sci. Eng., C* 38, 186–191.
- Guanghan, L., Min, Y., Qifang, Z., Ailan, W., Zexiang, J., 1995. Anodic stripping voltammetry for the determination of trace iodide. *Electroanalysis* 7, 591–593.

- Gupta, V.K., Singh, A.K., Kumawat, L.K., Mergu, N., 2016. An easily accessible switch-on optical chemosensor for the detection of noxious metal ions Ni(II), Zn(II), Fe(III) and UO₂(II). *Sens. Actuat., B* 222, 468–482.
- Hrobarikova, V., Hrobarik, P., Gajdos, P., Fitolis, I., Fakis, M., Persephonis, P., Zahradnik, P., 2010. Benzothiazole-based fluorophores of donor-pi-acceptor-pi-donor type displaying high two-photon absorption. *J. Org. Chem.* 75 (9), 3053–3068.
- Kaur, I., Khajuria, A., Ohri, P., Kaur, P., Singh, K., 2018. Benzothiazole based schiff-base-A mechanistically discrete sensor for HSO₄⁻ and I⁻: Application to bioimaging and vapour phase sensing of ethylacetate. *Sens. Actuators, B* 268, 29–38.
- Keshav, K., Torawane, P., Kumawat, M.K., Tayade, K., Sahoo, S.K., Srivastava, R., Kuwar, A., 2017. Highly selective optical and reversible dual-path chemosensor for cyanide detection and its application on live cells imaging. *Biosens. Bioelectron.* 92, 95–100.
- Kumar, P., Kim, K.-H., Bansal, V., Lazarides, T., Kumar, N., 2017. Progress in the sensing techniques for heavy metal ions using nanomaterials. *J. Ind. Eng. Chem.* 54, 30–43.
- Leonat, L., Sbârcea, G., Brânzoi, I.V., 2013. Cyclic voltammetry for energy levels estimation of organic materials. *UPB. Sci. Bull. Series B75* (3), 111–118.
- Li, J., Chen, Y., Chen, T., Qiang, J., Zhang, Z., Wei, T., Zhang, W., Wang, F., Chen, X., 2018. A benzothiazole based fluorescent probe for the efficient detection and discrimination of Zn²⁺ and Cd²⁺, using cysteine as an auxiliary reagent. *Sens. Actuators, B* 268, 446–455.
- Lv, S., Zhang, K., Zhu, L., Tang, D., 2020. ZIF-8-assisted NaYF₄:Yb, Tm@ZnO converter with exonuclease III-powered DNA walker for near-infrared light responsive biosensor. *Anal. Chem.* 92 (1), 1470–1476.
- Manna, A.K., Rout, K., Chowdhury, S., Patra, G.K., 2019. A dual-mode highly selective and sensitive Schiff base chemosensor for fluorescent colorimetric detection of Ni²⁺ and colorimetric detection of Cu²⁺. *Photochem. Photobiol. Sci.* 18 (6), 1512–1525.
- Manuela, M., Raposo, M., Cidalia, M., Castro, R., Mauricio, A., Fonseca, C., Schellenberg, P., Belsley, M., 2011. Design, synthesis, and characterization of the electrochemical, nonlinear optical properties, and theoretical studies of novel thienylpyrroleazo dyes bearing benzothiazole acceptor groups. *Tetrahedron* 67, 5189–5198.
- Maradiya, H.R., 2012. Disperse dyes based on 2-aminothiazole derivatives for cellulose triacetate fabric. *J. Saudi Chem. Soc.* 16 (1), 69–74.
- Ni, Y., Liu, H., Xu, J., Yue, Y., Shao, S., 2017. Construction of a selective electrochemical sensing solid-liquid interface for the selective detection of fluoride ion in water with bis(indolyl) methane-functionalized multi-walled carbon nanotubes. *New J. Chem.* 41, 14246–14252.
- Özkütük, M., İpek, E., Aydın, B., Mamaş, S., Seferoğlu, Z., 2016. Synthesis, spectroscopic, thermal and electrochemical studies on thiazolyl azo based disperse dyes bearing coumarin. *J. Mol. Struct.* 1108, 521–532.
- Padghan, S.D., Bhosale, R.S., Ghule, N.V., Puyad, A.L., Bhosale, S.V., Bhosale, S.V., 2016. Hydrogen sulfate ion sensing in aqueous media based on fused pyrimido benzothiazole derivative. *RSC Adv.* 6 (41), 34376–34380.
- Panitsiri, A., Tongkhan, S., Radchatawedchakoon, W., Sakee, U., 2016. Synthesis and anion recognition studies of novel bis (4-hydroxycoumarin) methane azo dyes. *J. Mol. Struct.* 1107, 14–18. <https://doi.org/10.1016/j.molstruc.2015.11.013>.
- Pan, Y., Huang, J., Han, Y., 2017. A new ES IPT-based fluorescent probe for highly selective and sensitive detection of HClO in aqueous solution. *Tetrahedron Lett.* 58 (13), 1301–1304.
- Rastegarzadeh, S., Pourreza, N., Saeedi, I., 2009. An optical redox chemical sensor for determination of iodide. *Talanta* 77 (3), 1032–1036.
- Sharma, H., Singh, N., Jang, D.O., 2015. A benzimidazole/benzothiazole-based electrochemical chemosensor for nanomolar detection of guanine. *RSC Adv.* 5 (9), 6962–6969.
- Shu, J., Tang, D., 2020. Recent advances in photoelectrochemical sensing: from engineered photoactive materials to sensing devices and detection modes. *Anal. Chem.* 92 (1), 363–377.
- Souza, F.C., Silva, D.A.I.D., Ribeiro, M.S., Faria, R.B., Melo, M.A., Toledo, R.M.M., D'Elia, E., 2013. A comparison of amperometric and spectrophotometric methods for the iodide concentration measurement: a tracer in produced water from offshore oil reservoirs. *J. Braz. Chem. Soc.* 24 (10), 1582–1591.
- Su, Z., Zhuang, H., Liu, H., Li, H., Xu, Q., Lu, J., Wang, L., 2014. Benzothiazole derivatives containing different electron acceptors exhibiting totally different data-storage performances. *J. Mater. Chem. C* 2 (28), 5673–5680.
- Vashisht, D., Kaur, K., Jukaria, R., Vashisht, A., Sharma, S., Mehta, S.K., 2019. Colorimetric chemosensor based on coumarin skeleton for selective naked eye detection of cobalt(II) ion in near aqueous medium. *Sens. Actuators, B* 280, 219–226.
- Vidya, B., Iniya, M., Sivaraman, G., Sumesh, R.V., Chellappa, D., 2017. Diverse benzothiazole based chemodosimeters for the detection of cyanide in aqueous media and in HeLa cells. *Sens. Actuators, B* 242, 434–442.
- Xiong, J., Sun, L., Liao, Y., Li, G.-N., Zuo, J.-L., You, X.-Z., 2011. A new optical and electrochemical sensor for fluoride ion based on the functionalized boron-dipyrromethene dye with tetrathiafulvalene moiety. *Tetrahedron Lett.* 52 (46), 6157–6161.
- Zeng, S., Li, S.-J., Sun, X.-J., Li, M.-Q., Xing, Z.-Y., Li, J.-L., 2019. A benzothiazole-based chemosensor for significant fluorescent turn-on and ratiometric detection of Al³⁺ and its application in cell imaging. *Inorganica Chimica Acta* 486, 654–662.